Desalination and Water Treatment
www.deswater.com

doi:10.5004/dwt.2017.20796

79 (2017) 178–187
June

Graphene oxide as a novel adsorbent for highly efficient removal of UO_2^{2+} from water

Baowei Hu[a], Qingyuan Hu[b], Xue Li[b,*], Hui Pan[b], Chengcai Huang[a], Chengguang Chen[b]

[a]*School of Life Science, Shaoxing University, Huancheng West Road No. 508, Zhejiang 312000, China, email: hbw@usx.edu.cn (B. Hu), 13157556371@126.com (C. Huang)*
[b]*College of Yuanpei, Shaoxing University, Qunxian Middle Road No. 2799, Zhejiang 312000, China, email: QinyuanHu32@126.com (Q. Hu), Tel. +86 13858480289, email: lixue.213@usx.edu.cn, 81850609@qq.com (X. Li), panhui@usx.edu.cn (H. Pan), 80167954@qq.com (C. Chen)*

Received 31 October 2016; Accepted 5 April 2017

ABSTRACT

In this paper, the use of graphene oxide (GO), high efficiency and low-risk adsorbent, has been studied for the removal of UO_2^{2+} from aqueous solutions. A series of experiments was conducted in a batch system to assess the effect of the system variables, i.e. contact time, initial pH, ionic strength, temperature, solid concentration and humic substances. The results indicated that the uptake is strongly dependent on pH but independent of ionic strength. A stimulative effect of HA/FA on UO_2^{2+} uptake was found at pH < 7.0, whereas inhibitory effect was observed at pH > 7.0. The adsorption kinetics of UO_2^{2+} uptake on GO was found to follow pseudo-second-order rate kinetic model very well, with a good correlation ($R^2 > 0.99$), indicating that the chemical adsorption was the rate-limiting step. The Linear, Langmuir, Freundlich, and Dubinin–Redushkevich (D–R) isotherms were used to analyze the equilibrium data at different temperatures, and the Langmuir isotherm model fits the sorption isotherms significantly better than the other three models. The maximum uptake capacity (q_{max}) reached 2.3532×10^{-4} mol·g^{-1} at 338 K, it is estimated by Langmuir. The thermodynamic analysis derived from temperature dependent uptake isotherms suggests that the uptake process of UO_2^{2+} on GO is spontaneous and endothermic. Results also showed that the GO was favourable adsorbent for UO_2^{2+}.

Keywords: Graphene oxide; Uranium; Absorption; Isotherm; Water

1. Introduction

With the rapid development of nuclear industry, excessive amounts of uranium have been discharged into the soil and water environment through various processes such as ore mining, nuclear fuel production, nuclear power generation, nuclear weapon manufacturing, and etc [1–3]. Uranium presents naturally as U isotopes, ^{238}U (99.28%), ^{234}U (0.006%) and ^{235}U (0.711%). It exists as a stable, soluble, hexavalent uranyl complex UO_2^{2+}, and poses the great risk to human health [4]. The drinking water guideline recommended by the United States Environmental Protection Agency (EPA) is 0.03 mg L^{-1}. The permissible discharge levels for nuclear industries range from 0.1 to 0.5 mg L^{-1} [5]. The disposed uranium can be eventually ingested by human beings due to the biological accumulation of food chain which can trigger toxicological effects and serious diseases such as spasm, diarrhea, lymphatolysis, thyroiditis, nephritis, hepatitis, neurological disorder and even cancers [6–10]. In view of this, it is urgent to seek advanced remediation strategies and high-effective adsorbent materials for the purification of UO_2^{2+}-bearing radioactive wastewaters.

Several strategies are available for the removal of UO_2^{2+} ions from aqueous solutions including solvent extraction, micellar ultrafiltration, chemical precipitation, organic and inorganic ion exchangers and adsorption [11]. Among these, the adsorption strategy is considered to be very important due to its diverse advantages such as cost effective treatment, ease of operation, narrow space for building

*Corresponding author.

the plant, no chemical reagents needed and no sludge produced. Recently, numerous studies have been investigated the adsorption of UO_2^{2+} on a variety of adsorbents such as nano-Fe^0 [12], sepiolite [13], hematite [14], Na-bentonite [15], fungus-attapulgite [16], cross-linked chitosan [17], bacillus subtilis [18], b-cyclodextrin-$Al(OH)_3$ [19], fungus-Fe_3O_4 [20], humic acid-immobilized zirconium-pillared clay [5], glycidyl methacrylate chelating resins [21], oxidized multiwalled carbon nanotubes [22], aluminum co-precipitated with goethite [23], etc. The interaction mechanism of uranium with adsorbent is evaluated from different experimental data such as the sorption curves at different experimental conditions, modeling simulation of sorption curves, and analysis of the spectra, which is mainly dominated by ion exchange or outer-sphere surface complexation at low pH, as well as the inner-sphere surface complexation or (co)precipitation at high pH values [24]. However, these materials suffer from either low sorption capacities or poor efficiencies, which limit their applications in the efficient removal of UO_2^{2+} from aqueous solutions in environmental pollution management. So, researches concerning to seeking novel potential adsorbents for the removal of UO_2^{2+} and related radionuclides with much higher adsorption capacities and efficiencies are always necessary.

Graphene oxide (GO), a novel 2D nanomaterial prepared from natural graphite, has recently attracted significant attention as a high adsorbent in wastewater treatment. GO exhibits an extremely large surface area to mass ratio and a high concentration of covalently bonded functional groups, including epoxide, ketone, and hydroxyl groups on the basal planes, and carboxylic, lactol, and phenolic groups at the edges [25–28]. It is demonstrated that GO exhibited larger adsorption capacities for heavy metals than any other currently reported material such as commercial granular active carbon and carbon nanotubes [29–32]. We also studied the adsorption of Cu(II) and Ni(II) on GO as a function of solution chemistry which showed an outstanding capability [33,34].

Hence, in order to extend the practical application of GO in radionuclides remediation, the objectives of this research were (1) to investigate the effect of water chemistry (e.g., reaction time, pH, ionic strength, initial solid content concentration and temperature) on UO_2^{2+} adsorption onto GO by batch techniques, (2) to study the adsorption of UO_2^{2+} on GO in the presence of humic acid (HA) or fulvic acid (FA), and (3) to determine the adsorption mechanism of UO_2^{2+} on GO. The highlights of this paper is that to evaluate an efficient and inexpensive adsorbent the potential application of GO towards the removal of radionuclides from aqueous solutions in environmental remediation strategy.

2. Experimental section

2.1. Chemicals and adsorbent preparation

All reagents used in the experiments were purchased in analytical purity and used without any purification. All solutions were prepared with Milli-Q water. Graphene oxide (GO) were prepared by using the modified Hummers method [33–35] from the natural flake graphite using concentrated H_2SO_4, $KMnO_4$ to oxidize the graphite layer. With the aid of ultrasonication, the oxidized graphite layers were exfoliated from each other. Then 30% H_2O_2 was added in the suspension to eliminate the excess MnO_4^-. The desired products were rinsed with deionized water. UO_2^{2+} stock solution was prepared by dissolving uranyl nitrate hexahydrate ($UO_2(NO_3)_2{\cdot}6H_2O$) in Milli-Q water. The solution was transferred to a 1,000 mL volumetric flask and diluted to the mark with distilled water to produce a uranium(VI) stock solution (1 $mg{\cdot}mL^{-1}$). The uranium solutions were prepared by diluting the stock solution to appropriate volumes depending upon the experimental requirements. The humic acid (HA) and fulvic acid (FA), which were obtained as a gift from the Institute of Plasma Physics, Chinese Academy of Sciences, were extracted from the soil of Hua-Jia county (Gansu province, China) and had been characterized in detail previously [36,37].

2.2. Batch adsorption experiments

All the adsorption experiments of UO_2^{2+} on GO were performed using batch technique in the polyethylene centrifuge tubes under T = 298, 318 and 338 K. In order to achieve homogeneous dispersion of GO and $NaClO_4$, the stock suspension of GO and $NaClO_4$ solution were first sonicated for 1 d in an ultrasonic bath before use. Then, appropriate amounts of UO_2^{2+} stock solution and FA or HA stock solution were added to achieve the desired concentrations of different components. The pH values of suspensions were adjusted to deserved pH values by adding ignore volume 0.01–1.0 $mol{\cdot}L^{-1}$ NaOH or $HClO_4$ solutions. After the samples placed on a reciprocating shaker table were shaken for two days, the solid and liquid phases were separated by centrifugation at 9000 rpm for 60 min at temperature controlled same to the uptake experiments. An aliquot of the supernatant was withdrawn and immediately filtered. It was necessary to emphasize that the adsorption of UO_2^{2+} on the tube wall was negligible according to the test of UO_2^{2+} sorption in the absence of GO. The concentration of U(VI) in the supernatant was analyzed by Arsenazo III spectrophotometric method at wavelength of 650 nm. The adsorption percentage (%) and the amounts of UO_2^{2+} adsorbed on GO (q_e) are calculated from the following equations, respectively [38].

$$\text{Adsorption percentage (\%)} = \frac{C_0 - C_e}{C_0} \times 100\% \quad (1)$$

$$q_e = \left(C_0 - C_e\right)\frac{V}{m} \quad (2)$$

where C_0 ($mol{\cdot}L^{-1}$) is the initial concentration of UO_2^{2+} in suspension, C_e ($mol{\cdot}L^{-1}$) is the concentration in supernatant after centrifugation, q_e ($mol{\cdot}L^{-1}$) is the concentration of UO_2^{2+} adsorbed on GO, m (g) is the mass of GO, and V is the volume of the suspension.

3. Results and discussion

3.1. Characterization of GO

Fig. 1A shows the SEM images of the GO samples, which indicated a disordered solid of GO made up from

thin, aggregated, and crumpled sheets. The TEM (Fig. 1B) images which demonstrate a two-dimensional multilayered structure with lateral sizes of several nanometers. The functional groups on the GO were examined by the FT-IR spectroscopy, as shown in Fig. 1C. GO has characteristic peaks of –OH stretching at 3387 cm^{-1}, C=O stretching at 1730 cm^{-1}, C=C stretching at 1624 cm^{-1}, C–OH stretching at 1400 cm^{-1}, and C–O–C and C–O stretching at 1173 cm^{-1}, 1054 cm^{-1}, respectively [24,39]. Different functional groups are found which indicating that the successful production of GO.

3.2. Adsorption dynamics

To investigate the dynamics of adsorption, the uptake of UO_2^{2+} on GO as a function of contact time is depicted in Fig. 2. As can be seen from Fig. 2A, once contacted, UO_2^{2+} could be adsorbed to GO rapidly during the first contact time of 6 h and then the sorption remained constant as time increasing. Two-step uptake process of UO_2^{2+} on GO conform to the general behavior of metal ion sorption at solid-water interfaces [40,41]. The interaction of UO_2^{2+} with surface sites of GO is fast, and then the slow continued UO_2^{2+} sorption on GO includes sorption of UO_2^{2+} ions onto sites that have relatively large activation energies, diffusion into the micropores of GO, and a continuous growth of a surface precipitate [42–44]. The result also suggests that 6 h is enough to achieve the sorption equilibrium of UO_2^{2+} on GO, so, 12 h were chosen to achieve the sorption equilibrium in the following experiments.

To help deduce the uptake mechanisms, the pseudo-second-order kinetic models were applied to simulate the experimental dynamic data of UO_2^{2+} on GO, which were expressed as [45,46]

$$\frac{t}{q_t} = \frac{1}{2kq_e^2} + \frac{t}{q_e} \tag{3}$$

Here q_t (mg·g^{-1}) is the amount of U(VI) uptake on GO at time t (h), q_e (mg·g^{-1}) is the equilibrium UO_2^{2+} capacity, and k (g·mg^{-1}·h^{-1}) is the rate constant of an uptake process. The straight-line plots of t/q_t versus t is shown in the inserted figure of Fig. 2B. The values of k and q_e determined from the slopes and intercepts of the kinetic model are listed in Table 1. The quick sorption of UO_2^{2+} on GO by large k (3.91 × 10^{-3} g·mol^{-1}·h^{-1}) suggests that it is dominated by chem-

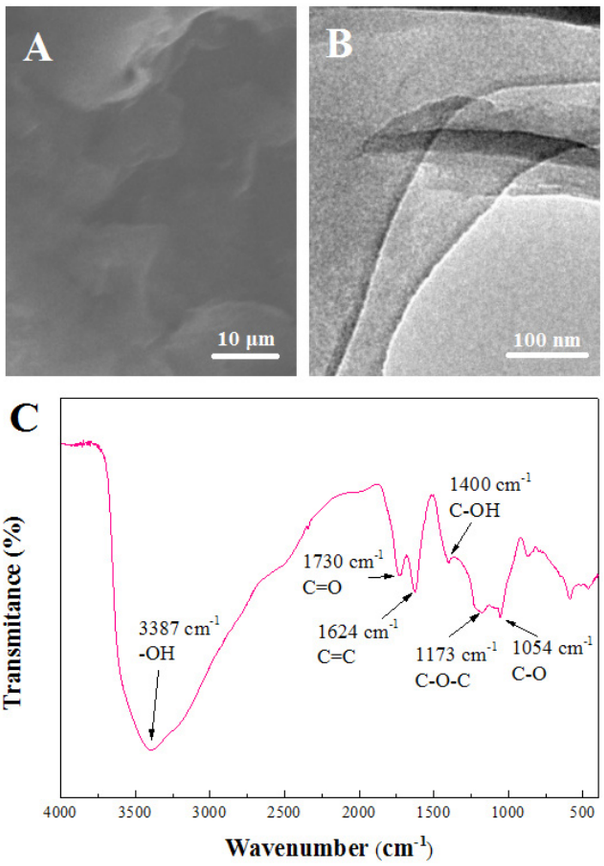

Fig. 1. (A) SEM images, (B) TEM images and (C) FTIR spectrum of GO.

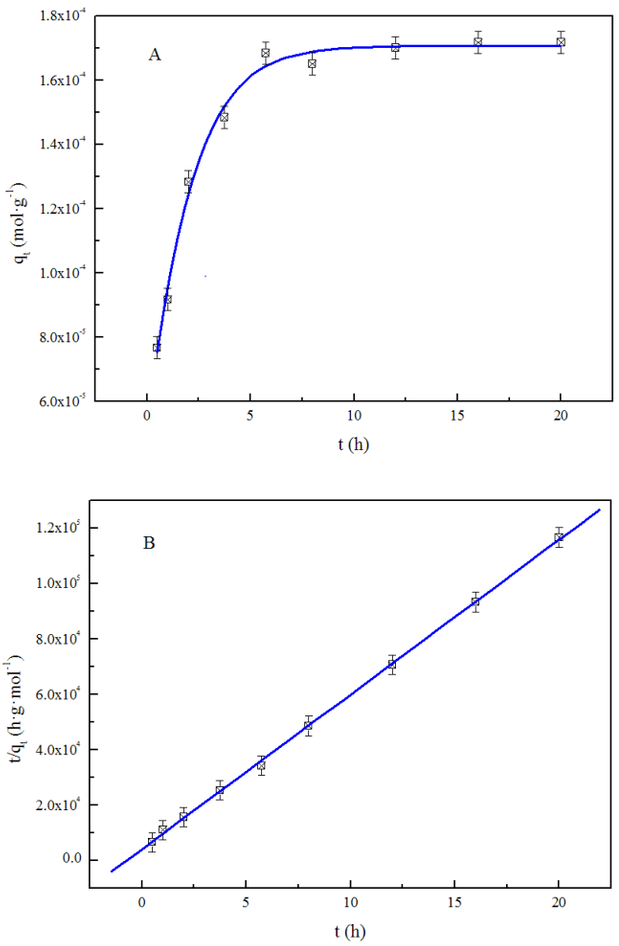

Fig. 2. Adsorption of UO_2^{2+} on GO as a function of contact time (A), Plot of t/q_t vs. t for the Pseudo-second-order rate calculation of UO_2^{2+} adsorption on GO (B), T = 298 K, pH = 6.0 ± 0.1, C (UO_2^{2+})$_{initial}$ = 2 × 10^{-5} mol·L^{-1}, I = 0.01 mol·L^{-1} $NaClO_4$, m/V = 0.1 g·L^{-1}.

Table 1
Kinetic parameters of UO_2^{2+} adsorption on GO

GO (g/L)	Pseudo-second-order parameters		
	q_e (mol·g^{-1})	k (g·mol^{-1}·h^{-1})	R^2
0.1	1.7906×10^{-4}	3.9103×10^{-3}	0.9997

ical sorption/surface complexation rather than physical sorption [47]. The correlation coefficient of the pseudo-second-order rate equation for the linear plot is 0.9997, which suggests that the kinetic uptake can be described by the pseudo-second order rate equation very well.

3.3. Effect of solid content

Fig. 3 reflects the effect of adsorbent concentration on the percentage removal of UO_2^{2+} on GO under equilibrium conditions. The distribution coefficient (K_d), values as a function of the GO content is also plotted in Fig. 3, was calculated from the concentration of UO_2^{2+} in suspension (C_0) and that of which in supernatant (C_e) according to the following equation:

$$K_d = \frac{C_0 - C_e}{C_e}\frac{V}{m} \quad (4)$$

One can see that the adsorption percentage of UO_2^{2+} increases from ~20% at m/V = 0.2 g/L to ~83% at m/V = 1.8 g/L. It is well known that the amount of functional groups at GO surfaces increases with increasing solid content. Thereby, more surface sites are available for the binding of UO_2^{2+} at higher solid contents. As can be seen from Fig. 3, the K_d values are nearly constant with increasing solid content. This phenomenon is consistent with the physicochemical properties of K_d values, i.e., the K_d value is independent of solid content and solution concentration when both of them are low [41,42]. At the same time, this illustrates that aggregation of adsorbent has not occurred whin the adsorption process of UO_2^{2+} on GO.

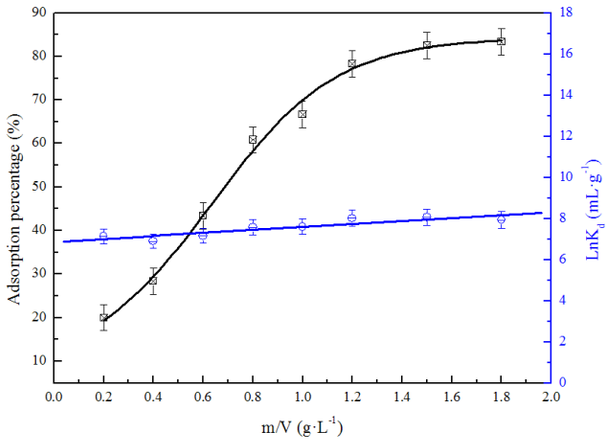

Fig. 3. Adsorption of UO_2^{2+} on GO as a function of solid content at T = 298 K, pH = 6.0 ± 0.1, $C(UO_2^{2+})_{initial} = 2 \times 10^{-5}$ mol·L^{-1}, I = 0.01 mol·L^{-1} $NaClO_4$.

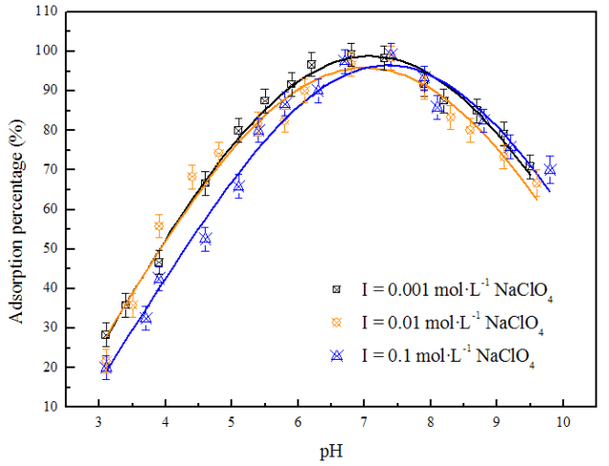

Fig. 4. The role of pH and ionic strength in UO_2^{2+} adsorption on GO, T = 298 K, $C(UO_2^{2+})_{initial} = 2 \times 10^{-5}$ mol·L^{-1}, m/V = 0.1 g·L^{-1}.

3.4. Impact of pH and ionic strength

Aqueous solution pH was the most important factor influencing the sorption of UO_2^{2+} by the change of surface properties of GO and formation of uranium species in aqueous solution. Fig. 4 shows the effect of pH on the adsorption of UO_2^{2+} on GO in the presence of 0.001 mol/L, 0.01 mol/L, 0.1 mol/L $NaClO_4$ solutions, respectively. The increased adsorption of UO_2^{2+} on GO was observed at pH 3.0–7.0, then descended adsorption of UO_2^{2+} on GO was observed at pH > 7.0. Approximately 99% of UO_2^{2+} was removed by GO at pH 7.0. Sun et al. demonstrated that GO presented the negative charge at pH > 2.0 [32]. So, the surface charge is negative because of the deprotonation reaction and the positive UO_2^{2+} ions are easily adsorbed on the negatively charged GO surfaces through electrostatic attraction. It is reasonable for the increased sorption of UO_2^{2+} on GO at high pH values, because of the imagination is more obvious with the increase pH. But, Sachs et al. [50] reported that the soluble carbonate complexes of UO_2^{2+} are the dominant anion species of $UO_2(CO_3)_3^{2-}$ and $UO_2(CO_3)_3^{4-}$ in the pH range of 7.0–10.0, these two complexes exist in various ratios depending on the pH of the solution. So, when pH > 7.0, the GO surface will be negatively charged and arise electrostatic repulsion with $UO_2(CO_3)_3^{2-}$ and $UO_2(CO_3)_3^{4-}$, the greater the repulsive force with the higher the pH, thereby the sorption of U(VI) decreased with increasing pH. Therefore the increased adsorption of UO_2^{2+} on GO could be attributed the strong electrostatic attraction between negative charged GO surface and positive charged of UO_2^{2+} species at pH < 7.0, but it is electrostatic repulsion at pH > 7.0. The effect of ionic strength on UO_2^{2+} adsorption on GO is also shown in Fig. 4. We can see that the adsorption of UO_2^{2+} on GO is weakly affected by ionic strength at pH < 7 and no effect is approximately found at pH > 7. Based on these conclusions, it can be deduced that the adsorption of UO_2^{2+} on GO is main dominated by inner-sphere complexation.

3.5. Impact of humic substances

The sorption behavior of UO_2^{2+} on GO is affected by its speciation in solution. Fig. 5 shows the sorption of UO_2^{2+} on GO as a function of pH in the presence and absence of HA and FA. At pH < 6.5, the presence of HA or FA enhances the sorption of U(VI) UO_2^{2+} on GO drastically, whereas the presence of HA or FA abates the sorption of U(VI) UO_2^{2+} on GO a certain extent, and there is no obvious gap between the two at the whole pH range. In the earlier study [34], we carried out an experiment about the uptake of HA or FA on GO as a function of solution pH, and we found that ~95% HA or FA can be adsorbed on GO at pH < 6.5, and then the uptake of HA or FA on GO decreases with pH increasing. We also determined the zeta potentials of HA or FA as a function of solution pH, respectively, and found that both HA and FA were negatively-charged with pH ranging from 3.0 to 10.0. So, at low pH, HA or FA with negative charge can be easily adsorbed on GO surfaces with positive charge due to electrostatic attraction, the strong binding ability of surface adsorbed HA or FA with UO_2^{2+} leads to the enhancement of UO_2^{2+} uptake on GO. However, at high pH, the uptake of HA or FA with negative charge on GO surfaces with negative charge becomes difficult due to electrostatic repulsion, so, the HA or FA in solution forms soluble complexes of HA- UO_2^{2+} or FA- UO_2^{2+}, resulting in the decrease of UO_2^{2+} uptake on GO. In previous investigations, Zhu et al. [51] studied the adsorption of UO_2^{2+} on Na-attapulgite in the absence and presence of HA, Niu et al. [52] studied HA effects on the sorption behavior of UO_2^{2+} uptake onto attapulgite. These results are similar to the previous work.

3.6. Sorption isotherms and thermodynamic study

The adsorption mechanism can be further understood by exploring the adsorption isotherms to describe the amount of UO_2^{2+} adsorption versus the equilibrium concentration, which can illustrate the adsorption efficiency, how the adsorption system proceeds, etc [39]. The related adsorption isotherms for UO_2^{2+} on GO at 298, 318 and 338 K were plotted in Fig. 6. It is clear that the uptake isotherm is the highest at T = 338 K and is the lowest at T = 298 K, indicates that the sorption is enhanced at higher temperature. This might be attributed to the following reasons [53–55]: (1) the changes of the pore sizes and the surface site number of GO might be increased with the increase of temperature; (2) the increase of temperature will lead to the increase of activity and proportion of UO_2^{2+} ions in solution, hence, increases the affinity of UO_2^{2+} to the adsorbent particles, or the charge and the potential of GO. The diffusion of UO_2^{2+} from the GO surface into GO pores may increase at high temperature. The isotherms of UO_2^{2+} adsorption on GO under different temperatures were plotted in Fig. 7 by fitting with four different models, viz. Linear, Langmuir, Freundlich and D-R, which can be expressed as Eqs. (5)–(8), respectively [56–58].

$$q_e = AC_e + B \tag{5}$$

$$q_e = \frac{bq_{\max}C_e}{1+bC_e} \tag{6}$$

$$q_e = k_F C_e^n \tag{7}$$

$$q_e = q_{\max}\exp\left(-\beta\varepsilon^2\right) \tag{8}$$

where q_e (mol·g^{-1}) is the amount of UO_2^{2+} adsorbed on per weight unit of GO after equilibrium, C_e (mol·L^{-1}) is the equilibrium concentration of UO_2^{2+} remained in the solution, A and B is the Linear constant, $q_{\max}$ (mol·g^{-1}) is the maximum uptake capacity, b (L·mol^{-1}) is a Langmuir constant that relates to the heat of uptake, k_F (mol^{1-n}·L^n·g^{-1}) and n is the Langmuir constants, k_F represents the uptake capacity when UO_2^{2+} equilibrium concentration equals to 1, and n represents the degree of dependence of uptake with equilibrium concentration, β (mol^2·kJ^{-2}) is the activity coefficient related to mean uptake energy, and ε is the Polanyi potential, which is equal to $\varepsilon = RT\ln\left(1+\frac{1}{C_e}\right)$, where R (8.3145

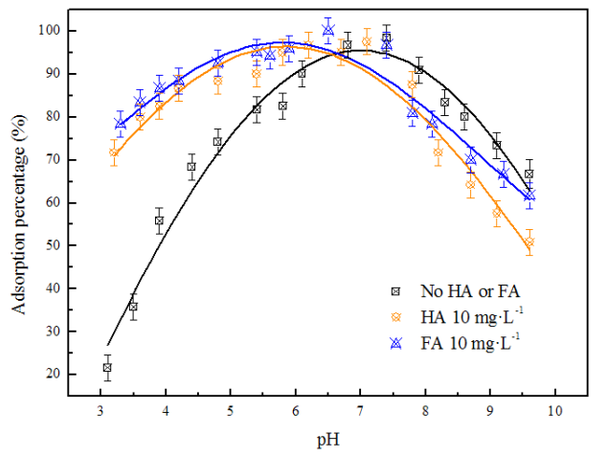

Fig. 5. The role of HA/FA in UO_2^{2+} adsorption on GO, T = 298 K, $C(UO_2^{2+})_{initial}$ = 2 × 10^{-5} mol·L^{-1}, m/V = 0.1 g·L^{-1}, I = 0.01 mol·L^{-1} $NaClO_4$.

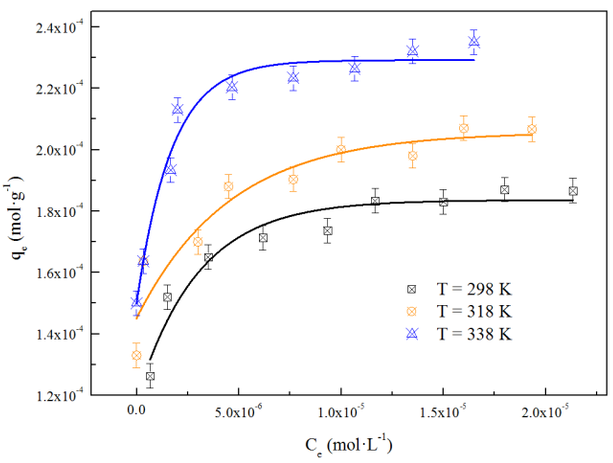

Fig. 6. Adsorption isotherms of UO_2^{2+} adsorption on GO at three different temperatures, pH = 6.0 ± 0.1, m/V = 0.1 g·L^{-1}, I = 0.01 mol·L^{-1} $NaClO_4$.

J·mol^{-1}·K^{-1}) is ideal gas constant , and T (K) is the absolute temperature in Kelvin, E (kJ·mol^{-1}) is defined as the free energy change, which requires to transfer 1 mol of UO_2^{2+} from solution to the GO surfaces, its value can be calculated from the following equation $E = \frac{1}{\sqrt{2\beta}}$.

The related parameters of four models were listed in Table 1. It is clear that the Langmuir isotherm model fits the sorption isotherms significantly better than the other three models, which is supported by the good correlation coefficients in Table 2. The q_{max} value increases from 1.9058 × 10^{-4} to 2.3532 × 10^{-4} mol·g^{-1} as temperature increases from 298 to 338 K, suggesting that high temperature is favorable to sorption. The results suggesting that the binding energy on the whole surface of GO is uniform. In other words, the whole surface has identical adsorption activity and therefore the adsorbed UO_2^{2+} on GO surface do not interact with each other, and they are adsorbed by forming an almost complete monolayer coverage of GO. A comparison as shown in Fig. 8 of the maximum uptake capacities of UO_2^{2+} on GO studied in this work with other adsorbents documented in the literature [22,59–63], which shows that the uptake capacity of UO_2^{2+} on GO is much higher than other. Thus GO can be used as an alternative material to uptake UO_2^{2+} from aqueous solution.

In order to investigate the thermodynamic properties, the sorption isotherms at three different temperatures are used to calculate the thermodynamic data. The thermodynamic parameters (i.e., Gibbs free energy ΔG^0, entropy ΔS^0, and enthalpy ΔH^0) for UO_2^{2+} uptake on GO can be determined from the temperature dependence. The ΔG^0 is calculated from the relationship.

$$\Delta G^0 = -RT \ln K^0 \quad (9)$$

where K^0 is the uptake equilibrium constant. Values of $\ln K^0$ obtained by plotting $\ln K_d$ versus C_e for uptake of UO_2^{2+} on GO (Fig. 9A) and extrapolating C_e to zero are 11.50 (T = 298 K), 11.87 (T = 318 K) and 12.14 (T = 338 K), respectively. The ΔS^0 evaluated from the slope which linear plot of ΔG^0 versus T is achieved according to the equation (Fig. 9B).

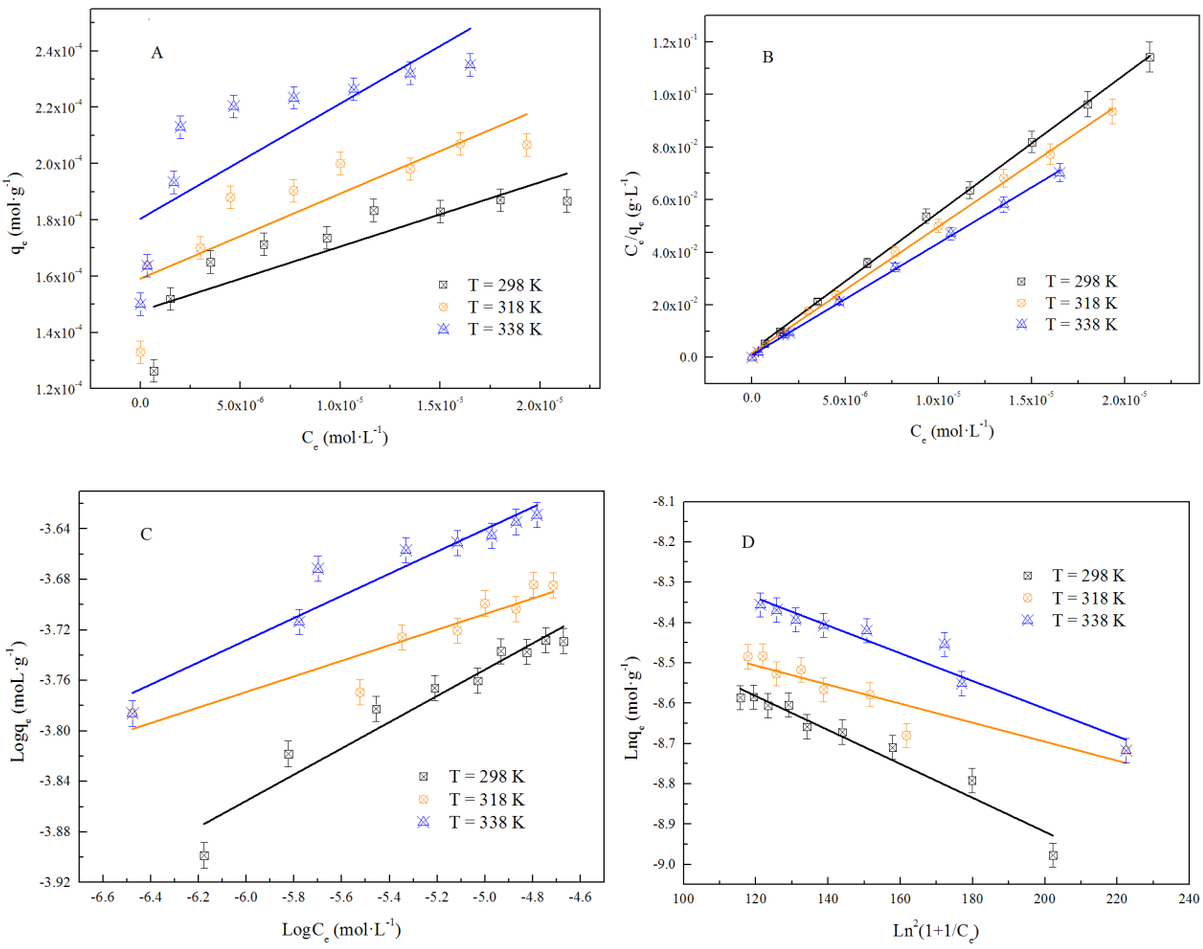

Fig. 7. Fitting results of Linear (A), Langmuir (B), Freundlich (C) and D-R (D) adsorption isotherms of UO_2^{2+} adsorption on GO at three different temperatures, pH = 6.0 ± 0.1, m/V = 0.1 g·L^{-1}, I = 0.01 mol·L^{-1} $NaClO_4$.

Table 2
The parameters for Linear, Langmuir, Freundlich and D-R isotherms of UO_2^{2+} adsorption on GO at different temperatures

Linear model	A		B	R^2
T = 298 K	1.4767×10^{-4}		2.2865	0.4562
T = 318 K	1.5911×10^{-4}		3.0228	0.4960
T = 338 K	1.8042×10^{-4}		4.0918	0.3622
Langmuir model	q_{max} (mol·g^{-1})		b (L·mol^{-1})	R^2
T = 298 K	1.9058×10^{-4}		1.9012×10^{6}	0.9985
T = 318 K	2.0812×10^{-4}		2.7457×10^{6}	0.9960
T = 338 K	2.3532×10^{-4}		4.3134×10^{6}	0.9984
Freundlich model	K_F (mol^{1-n}·L^n·g^{-1})		n	R^2
T = 298 K	5.8625×10^{-4}		0.1039	0.8613
T = 318 K	3.9891×10^{-4}		0.0617	0.7176
T = 338 K	6.2894×10^{-4}		0.0878	0.8288
D-R model	q_{max} (mol·g^{-1})	β (mol^2·kJ^{-2})	E (kJ·mol^{-1})	R^2
T = 298 K	3.1042×10^{-4}	6.8577×10^{-4}	27.0020	0.8910
T = 318 K	2.6817×10^{-4}	3.3759×10^{-4}	38.4851	0.6714
T = 338 K	3.6103×10^{-4}	4.3430×10^{-4}	33.9305	0.8639

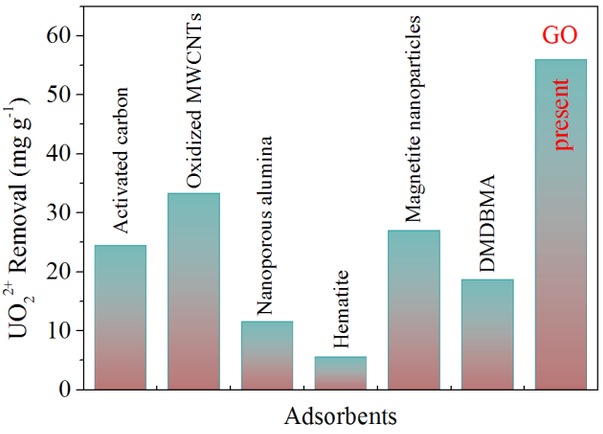

Fig. 8. A comparison of the maximum uptake capacities of UO_2^{2+} on GO with other adsorbents.

$$\left(\frac{\partial \Delta G^0}{\partial T}\right)_p = -\Delta S^0 \quad (10)$$

ΔH^0 is then calculated from the expression:

$$\Delta H^0 = \Delta G^0 + T\Delta S^0 \quad (11)$$

The values obtained from Eqs. (10) to (11) are tabulated in Table 3. A positive value of the ΔH^0 suggesting that the uptake of UO_2^{2+} on GO is endothermic, which is an indication of the existence of a strong interaction between UO_2^{2+} and GO. One possible explanation to this positive ΔH^0 is that UO_2^{2+} ions are firstly to be stripped out (at least partially) of their hydration shell in the aqueous solutions, namely this process requires energy input. So, it is favored at high

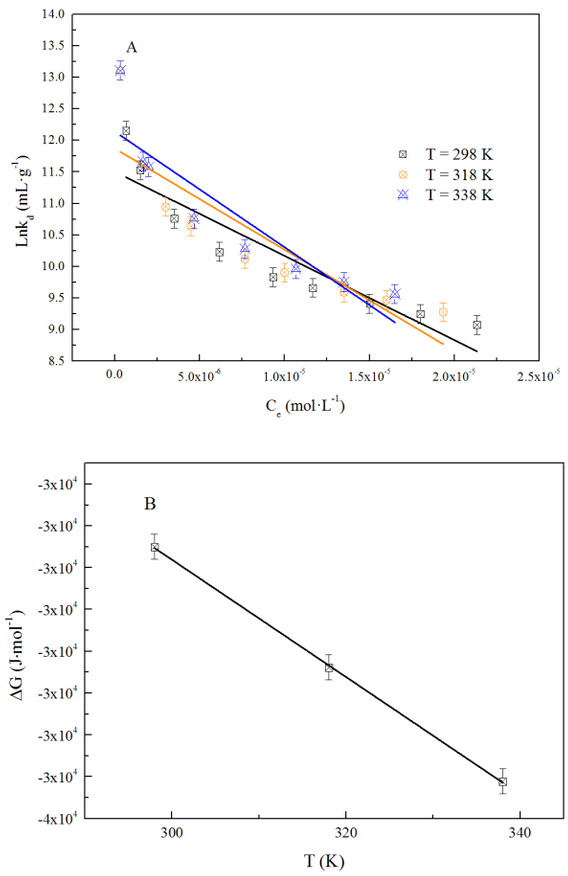

Fig. 9. The linear plot of LnK_d versus C_e (A) at three different temperatures and ΔG^0 versus T (B) for UO_2^{2+} adsorption on GO, pH = 6.0 ± 0.1, m/V = 0.1 g·L^{-1}, I = 0.01 mol·L^{-1} $NaClO_4$.

Table 3
Values of thermodynamic parameters for UO_2^{2+} adsorption on GO

T(K)	$\Delta G°$ (kJ·mol^{-1})	$\Delta S°$ (J·mol^{-1}·K^{-1})	$\Delta H°$ (kJ·mol^{-1})
298	–28.5016	140.3014	10.5313
318	–31.3876		10.2649
338	–34.1137		10.1585

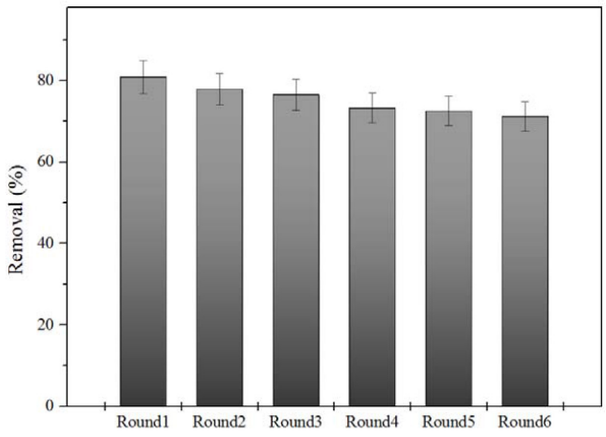

Fig. 10. Recycling for U(VI) uptake on GO, T = 298K, pH = 6.0 ± 0.1, m/V = 0.1 g·L^{-1}, I = 0.01 mol·L^{-1} $NaClO_4$.

temperature. The ΔG^0 is negative as expected for a spontaneous process under the conditions applied. The value of ΔG^0 becomes more negative with the increase of temperature, which indicates that the reaction is more favorable at higher temperatures. At high temperature, UO_2^{2+} are readily desolvated and hence its sorption becomes more favorable. The positive value of ΔS^0 implies some structural changes in UO_2^{2+} and GO during the uptake process, which leads to an increase in the disorderness of the GO-solution interfacial system during the uptake of UO_2^{2+} on GO. The thermodynamic analysis derived from temperature dependent uptake isotherms suggests that the uptake process of UO_2^{2+} on GO is spontaneous and endothermic.

3.7. Regeneration and reusability

The regeneration and reusability of GO was verified to evaluate its application potential in the purification of U(VI)-containing wastewater. The regenerated GO was used for six continuous sorption-desorption cycles. As shown in Fig. 10, the removal of U(VI) slightly decreases from 81% to 71% after six cycles, corresponding to a decreased sorption percentage of ~10%. Overall, the GO exhibits excellent recycling performance and can support long-term usage in the removal of U(VI) with favorable cost effectiveness. With more and more metal ions and radionuclides released into the natural environment, it is very important to treat these contaminants in water and soil [64–68]. The results obtained herein indicated that GO is a promising candidate in the nuclear waste management.

4. Conclusions

In this study, batch technique was adopted to investigate the uptake of UO_2^{2+} on GO as a function of various water chemistries such as contact time, pH, ionic strength, temperature, solid concentration and humic substances. The UO_2^{2+} adsorption capacity by GO was strongly dependent on contact time, pH, and solid content. The adsorption capacity of UO_2^{2+} onto GO increases with an increase of contact time and reaches adsorption equilibrium within 5 h, the adsorption removal efficiency increased with increasing pH to a maximum value at pH = 7.0 and then declines rapidly with further increase in pH. Thus, inner-sphere surface complexation is the main mechanism responsible for the uptake of Co(II) on GO. The uptake of Co(II) is influenced by HA/FA significantly, and the effect of HA/FA on UO_2^{2+} uptake is dependent on pH values. The presence of HA/FA enhances the uptake of Ni(II) on GO at low pH, while reduces UO_2^{2+} uptake on GO at high pH. Linear, Langmuir, Freundlich and D-R adsorption models were used for the mathematical description of the adsorption equilibrium. It is found that the adsorption of UO_2^{2+} onto GO correlated well with the Langmuir model as compared the other three models under the concentration range studied. Adsorption kinetics data were tested very well using the pseudo-second-order models, indicating that the chemical adsorption was the rate-limiting step. Results of this work are great importance for environmental application of GO in the treatment and indicated that GO was favorable adsorbent for UO_2^{2+} removal from aqueous solutions.

Acknowledgements

Financial supports from the Science and Technology Project of Shaoxing (2014B70041) are acknowledged.

References

[1] L.M. Camacho, S.G. Deng, R.R. Parra, Uranium removal from groundwater by natural clinoptilolite zeolite: effects of pH and initial feed concentration, J. Hazard. Mater., 175 (2010) 393–398.
[2] K. Maher, J.R. Bargar, G.E. Brown, Jr, Environmental speciation of actinides, Inorg. Chem., 52 (2013) 3510–3532.
[3] G.D. Sheng, J. Hu, A. Alsaedi, W. Shammakh, S. Monaquel, F. Ye, H. Li, Y.Y. Huang, A.S. Alshomrani, T. Hayat, B. Ahmad, Interaction of uranium(VI) with titanate nanotubes by macroscopic and spectroscopic investigation, J. Mol. Liq., 212 (2015) 563–568.
[4] S.C. Sheppard, W.G. Evenden, Bioavailability indices for uranium: effect of concentration in eleven soils, Arch. Environ. Con. Tox., 23 (1992) 117–124.
[5] T.S. Anirudhan, C.D. Bringle, S. Rijith, Removal of uranium(VI) from aqueous solutions and nuclear industry effluents using humic acid-immobilized zirconium-pillared clay, J. Environ. Radioactiv., 101 (2010) 267–276.
[6] D. Brugge, V. Buchner, Health effects of uranium: new research findings, Rev. Environ. Heal., 26 (2011) 231–249.
[7] P.F. Tang, J. Shen, Z.D. Hu, G.L. Bai, M. Wang, B.J. Peng, R.P. Shen, W.S. Linghu, High-efficient scavenging of U(VI) by magnetic Fe_3O_4@gelatin composite, J. Mol. Liq., 221 (2016) 497–506.
[8] S. Keith, O. Faroon, N. Roney, F. Scinicariello, S. Wilbur, L. Ingerman, F. Llados, D. Plewak, D. Wohlers, G. Diamond, Toxicological profile for uranium, Agency for Toxic Substances and Disease Registry (US), (2013) 39–175.

[9] Z. Hon, J. Österreicher, L. Navrátil, Depleted uranium and its effects on humans, Sustainability, 7 (2015) 4063–4077.
[10] L. Stammler, A. Uhl, B. Mayer, F. Keller, Renal effects and carcinogenicity of occupational exposure to uranium: a meta-analysis, Nephron. Extra., 6 (2016) 1–11.
[11] J.R. Bargar, R. Reitmeyer, J.J. Lenhart, J.A. Davis, Characterization of U(VI)- carbonato ternary complexes on hematite: EXAFS and electrophoretic mobility measurements, Geochim. Cosmochim. Acta, 64 (2000) 2737–2749.
[12] C.C. Ding, W.C. Cheng, Y.B. Sun, X.K. Wang, Effects of Bacillus subtilis on the reduction of U(VI) by nano-Fe^0, Geochim. Cosmochim. Acta, 165 (2015) 86–107.
[13] Y.B. Sun, J.X. Li, X.K. Wang, The retention of uranium and europium onto sepiolite investigated by macroscopic, spectroscopic and modeling techniques, Geochim. Cosmochim. Acta, 140 (2014) 621–643.
[14] J.R. Bargar, R. Reitmeyer, J.J. Lenhart, J.A. Davis, Characterization of U(VI)-carbonato ternary complexes on hematite: EXAFS and electrophoretic mobility measurements, Geochim. Cosmochim. Acta, 64 (2000) 2737–2749.
[15] G.D. Sheng, X.Y. Shao, Y.M. Li, J.F. Li, H.P. Dong, W. Cheng, X. Gao, Y.Y. Huang, Enhanced removal of uranium(VI) by nanoscale zerovalent iron supported on Na-bentonite and an investigation of mechanism, J. Phys. Chem. A, 118 (2014) 2952–2958.
[16] W.C. Cheng, C.C. Ding, Y.B. Sun, X.K. Wang, Fabrication of fungus/attapulgite composites and their removal of U(VI) from aqueous solution, Chem. Eng. J., 269 (2015) 1–8.
[17] G.H. Wang, J.S. Liu, X.G. Wang, Z.Y. Xie, N.S. Deng, Adsorption of uranium (VI) from aqueous solution onto cross-linked chitosan, J. Hazard. Mater., 168 (2009) 1053–1058.
[18] T. Yao, X.W. Wu, X. Chen, Y.P. Xiao, Y.G. Zhang, Y.L. Zhao, F.B. Li, Biosorption of Eu(III) and U(VI) on Bacillus subtilis: macroscopic and modeling investigation, J. Mol. Liq., 219 (2016) 32–38.
[19] C.C. Ding, W.C. Cheng, Z.X. Jin, Y.B. Sun, Plasma synthesis of b-cyclodextrin/$Al(OH)_3$ composites as adsorbents for removal of UO_2^{2+} from aqueous solutions, J. Mol. Liq., 207 (2015) 224–230.
[20] C.C. Ding, W.C. Cheng, Y.B. Sun, Novel fungus-Fe_3O_4 bio-nanocomposites as high performance adsorbents for the removal of radionuclides, J. Hazard. Mater., 295 (2015) 127–137.
[21] A.M. Donia, A.A. Atia, E.M.M. Moussa, A.M. El-Sherif, M.O.A. El-Magied, Removal of uranium(VI) from aqueous solutions using glycidyl methacrylate chelating resins, Hydrometallurgy, 95 (2009) 183–189.
[22] Y.B. Sun, S.T. Yang, G.D. Sheng, Z.Q. Guo, X.K. Wang, The removal of U(VI) from aqueous solution by oxidized multiwalled carbon nanotubes, J. Environ. Radioactiv., 105 (2012) 40–47.
[23] Y.B. Sun, S.B. Yang, Q. Wang, A. Alsaedi, X.K. Wang, Sequestration of uranium on fabricated aluminum co-precipitated with goethite, Radiochim. Acta., 102 (2014) 797–804.
[24] X. Wang, Q. Fan, S. Yu, Z. Chen, Y. Ai, Y. Sun, A. Hobiny, A. Alsaedi, X. Wang, High sorption of U(VI) on graphene oxides studied by batch experimental and theoretical calculations, Chem. Eng. J., 287 (2016) 448–455.
[25] J.Y. Huang, Z.W. Wu, L.W. Chen, Y.B. Sun, Surface complexation modeling of adsorption of Cd(II) on graphene oxides, J. Mol. Liq., 209 (2015) 753–758.
[26] L.L. Fan, C.N. Luo, X.J. Li, F.G. Lu, H. Qiu, M. Sun, Fabrication of novel magnetic chitosan grafted with graphene oxide to enhance adsorption properties for methyl blue, J. Hazard. Mater., 215–216 (2012) 272–279.
[27] Y.B. Sun, Q. Wang, C.L. Chen, X.L. Tan, X.K. Wang, Interaction between Eu(III) and graphene oxide nanosheets investigated by batch and extended X-ray absorption fine structure spectroscopy and by modeling techniqus, Environ. Sci. Technol., 46 (2012) 6020–6027.
[28] C.C. Ding, W.C. Cheng, Y.B. Sun, X.K. Wang, Determination of chemical affinity of graphene oxide nanosheets with radionuclides investigated by macroscopic, spec-troscopic and modeling techniques, Dalton. Trans., 43 (2014) 3888–3896.
[29] Y.B. Sun, D.D. Shao, C.L. Chen, S.B. Yang, X.K. Wang, Highly efficient enrichment of radionuclides on graphene oxide supported polyaniline, Environ. Sci. Technol., 47 (2013) 9904–9910.
[30] Q. Wang, X.K. Wang, Z.F. Chai, W.P. Hu, Cheminform abstract: low-temperature plasma synthesis of carbon nanotubes and graphene based materials and their fuel cell applications, Chem. Soc. Rev., 42(23) (2013) 8821–8834.
[31] G.X. Zhao, L. Jiang, Y.D. He, J.X. Li, H.L. Dong, X.K. Wang, W.P. Hu, Sulfonated graphene for persistent aromatic pollutant management, Adv. Mater., 23 (2011) 3959–3963.
[32] Y.B. Sun, S.B. Yang, Y. Chen, C.C. Ding, W.C. Cheng, X.K. Wang, Adsorption and desorption of U(VI) on functionalized graphene oxides: a combined experimental and theoretical study, Environ. Sci. Technol., 49 (2015) 4255–4262.
[33] X. Li, M. Yu, Q. Lv, Y. Tan, Sequestration of Ni(II) onto graphene oxide from synthetic wastewater as affected by coexisting constituents, Desal. Water. Treat., 57 (2016) 20904–20914.
[34] X. Li, Y. Fang, X. Tang, Using graphene oxide as a superior adsorbent for the highly efficient immobilization of Cu(II) from aqueous solution, J. Mol. Liq., 199 (2014) 237–243.
[35] M. Hirata, T. Gotou, S. Horiuchi, M. Fujiwara, M. Ohba, Thin-film particles of graphite oxide 1: : High-yield synthesis and flexibility of the particles, Carbon, 42 (2004) 2929–2937.
[36] G. Sheng, R. Shen, H. Dong, Y. Li, Colloidal diatomite, radionickel and humic substance interaction: A combined batch, XPS and EXAFS investigation, Environ. Sci. Pollut. Res. Int., 20 (2013) 3708–3717.
[37] X. Tan, Q. Fan, X. Wang, B. Grambow, Eu(III) sorption to TiO_2 (anatase and rutile): batch, XPS, and EXAFS studies, Environ. Sci. Technol., 43 (2009) 3115–3121.
[38] H. Xu, J. Hu, X.M. Ren, G. Li, Macroscopic and microscopic insight into the mutual effects of europium(III) and phosphate on their interaction with graphene oxide, RSC. Adv., 6 (2016) 85046–85057.
[39] X. Liu, Y.S. Huang, S.X. Duan, Y.N. Wang, J.X. Li, Y.T. Chen, T. Hayat, X.K. Wang, Graphene oxides with different oxidation degrees for Co(II) ion pollution management, Chem. Eng. J., 302 (2016) 763–772.
[40] S. Lee, P.R. Anderson, G.B. Bunker, C. Karanfil, EXAFS study of Zn sorption mechanisms on montmorillonite, Environ. Sci. Technol., 38 (2004) 5426–5432.
[41] G.D. Sheng, S.T. Yang, J. Sheng, J. Hu, X.L. Tan, X.K. Wang, Macroscopic and microscopic investigation of Ni(II) sequestration on diatomite by batch, XPS, and EXAFS techniques, Environ. Sci. Technol., 45 (2011) 7718–7726.
[42] T.J. Strathmann, S.B. Myneni, Effect of soil fulvic acid on nickel(II) sorption and bonding at the aqueous-boehmite (gamma-AlOOH) interface, Environ. Sci. Technol., 39 (2005) 4027–4034.
[43] G.D. Sheng, J. Hu, H. Jin, S.T. Yang, X.M. Ren, J.X. Li, Y.X. Chen, X.K. Wang, Effect of humic acid, fulvic acid, pH, ionic strength and temperature on ^{63}Ni(II) sorption to MnO_2, Radiochim. Acta., 98 (2010) 291–299.
[44] S.T. Yang, G.D. Sheng, X.L. Tan, J. Hu, J.Z. Du, M. Gilles, X.K. Wang, Determination of Ni(II) uptake mechanisms on mordenite surfaces: A combined macroscopic and microscopic approach, Geochima. Cosmochim. Acta., 75 (2011) 6520–6534.
[45] Y.S. Ho, Review of second-order models for adsorption systems, J. Hazard. Mater., 136 (2006) 681–689.
[46] Y.S. Ho, G. McKay, Pseudo-second order model for sorption processes, Process. Biochem., 34 (1999) 451–465.
[47] Y.L. Chi, Y.T. Chen, X. Liu, Z.J. Guo, L.S. Cai, Impact of environmental conditions on the sorption behavior of UO_2^{2+} onto attapulgite studied by batch experiments, J. Radioanal. Nucl. Chem., 292 (2012) 1349–1355.
[48] J. Xiao, Y.T. Chen, W.H. Zhao, J.B. Xu, Sorption behavior of U(VI) onto Chinese bentonite: Effect of pH, ionic strength, temperature and humic acid, J. Mol. Liq., 188 (2013) 178–185.
[49] D.D. Shao, Z. Jiang, X. Wang, J. Li, Y. Meng, Plasma Induced Grafting Carboxymethyl Cellulose on Multiwalled Carbon Nanotubes for the Removal of UO_2^{2+} from Aqueous Solution, J. Phys. Chem. B., 113 (2009) 860–864.

[50] S. Sachs, G. Bernhard, Sorption of U(VI) onto an artificial humic substance-kaolinite-associate, Chemosphere, 72 (2008) 1441–1447.
[51] W.B. Zhu, Z.J. Liu, L. Chen, Y.H. Dong, Sorption of uranium(VI) on Na-attapulgite as a function of contact time, solid content, pH, ionic strength, temperature and humic acid, J. Radioanal. Nucl. Chem., 289 (2011) 781–788.
[52] Z.W. Niu, Q.H. Fan, W.H. Wang, J.Z. Xu, L. Chen, W.S. Wu, Effect of pH, ionic strength and humic acid on the sorption of uranium(VI) to attapulgite, Appl. Radiat. Isotopes., 67 (2009) 1582–1590.
[53] G.X. Zhao, J. Li, X.M. Ren, C.L. Chen, X.K. Wang, Few-layered graphene oxide nanosheets as superior sorbents for heavy metal ion pollution management, Environ. Sci. Technol., 45 (2011) 10454–10462.
[54] F. Partey, D. Norman, S. Ndur, R. Nartey, Arsenic sorption onto laterite iron concretions: temperature effect, J. Colloid. Interface. Sci., 321 (2008) 493–500.
[55] Z. Chen, S. Lu, Investigation of the effect of pH, ionic strength, foreign ions, temperature, soil humic substances on the sorption of $^{152+154}$Eu(III) onto NKF-6 zeolite, J. Radioanal. Nucl. Ch., 309 (2016) 717–728.
[56] G. Sheng, H. Dong, R. Shen, Y. Li, Microscopic insights into the temperature-dependent adsorption of Eu(III) onto titanate nanotubes studied by FTIR, XPS, XAFS and batch technique, Chem. Eng. J., 217 (2013) 486–494.
[57] G. Sheng, Y. Li, H. Dong, D. Shao, Environmental condition effects on radionuclide ^{64}Cu(II) sequestration to a novel composite: Polyaniline grafted multiwalled carbon nanotubes, J. Radioanal. Nucl. Ch., 293 (2012) 797–806.
[58] G. Sheng, H. Dong, Y. Li, Characterization of diatomite and its application for the retention of radiocobalt: role of environmental parameters, J. Environ. Radioact., 113 (2012) 108–115.
[59] A. Mellah, S. Chegrouche, M. Barkat, The removal of uranium(VI) from aqueous solutions onto activated carbon: kinetic and thermodynamic investigations, J. Colloid Interface Sci., 296 (2006) 434–441.
[60] Y. Sun, S. Yang, G. Sheng, Z. Guo, X. Tan, J. Xu, X. Wang, Comparison of U(VI) removal from contaminated groundwater by nanoporous alumina and nonnanoporous alumina, Sep. Purif. Technol., 83 (2011) 196–203.
[61] D.L. Zhao, X.B. Wang, S.T. Yang, Z.Q. Guo, G.D. Sheng, Impact of water quality parameters on the sorption of U(VI) onto hematite, J. Environ. Radioact., 103 (2012) 20–29.
[62] R. Leal, M. Yamaura, Equilibrium adsorption isotherm of U(VI) at pH 4 and pH 5 onto synthetic magnetite nanoparticles, Int. J. Nucl. Energ. Sci. Technol., 6 (2011) 1–7.
[63] D. Prabhakaran, M.S. Subramanian, Selective extraction of U(VI) Th(IV), and La(III) from acidic matrix solutions and environmental samples using chemically modified Amberlite XAD-16 resin, Anal. Bioanal. Chem., 379 (2004) 519–525.
[64] G. Sheng, J. Hu, H. Li, J. Li, Y. Huang, Enhanced sequestration of Cr(VI) by nanoscale zero-valent iron supported on layered double hydroxide by batch and XAFS study, Chemosphere, 148 (2016) 227–232.
[65] G. Sheng, S. Yang, Y. Li, X. Gao, Y. Huang, X. Wang, Retention mechanisms and microstructure of Eu(III) on manganese dioxide studied by batch and high resolution EXAFS technique, Radiochim. Acta., 102 (2014) 155–167.
[66] B. Hu, F. Ye, X. Ren, D. Zhao, G. Sheng, H. Li, J. Ma, X. Wang, Y. Huang (2016) X-ray absorption fine structure study of enhanced sequestration of U(VI) and Se(IV) by montmorillonite decorated zerovalent iron nanoparticles, Environ. Sci. Nano., DOI: 10.1039/C6EN00421K.
[67] G. Sheng, P. Yang, Y. Tang, Q. Hu, H. Li, X. Ren, B. Hu, X. Wang, Y. Huang, New insights into the primary roles of diatomite in the enhanced sequestration of UO_2^{2+} by zerovalent iron nanoparticles: An advanced approach utilizing XPS and EXAFS, Appl. Catal. B Environ., 193 (2016) 189–197.
[68] G. Sheng, A. Alsaedi, W. Shammakh, S. Monaquel, J. Sheng, X. Wang, H. Li, Y. Huang, Enhanced sequestration of selenite in water by nanoscale zero valent iron immobilization on carbon nanotubes by a combined batch, XPS and XAFS investigation, Carbon, 99 (2016) 123–130.